Hearing Research 343 (2017) 34–49

Contents lists available at ScienceDirect

Hearing Research

journal homepage: www.elsevier.com/locate/heares

Descending projections from the inferior colliculus to medial olivocochlear efferents: Mice with normal hearing, early onset hearing loss, and congenital deafness

Kirupa Suthakar [a, b, *], David K. Ryugo [a, b, c]

[a] Hearing Research Unit, Neuroscience Division, Garvan Institute of Medical Research, Darlinghurst, NSW, 2010, Australia
[b] School of Medical Sciences, Faculty of Medicine, UNSW Australia, Sydney, NSW, 2052, Australia
[c] Department of Otolaryngology, Head, Neck & Skull Base Surgery, St Vincent's Hospital, Sydney, NSW, 2010, Australia

ARTICLE INFO

Article history:
Received 12 April 2016
Received in revised form
20 June 2016
Accepted 24 June 2016
Available online 12 July 2016

Keywords:
Tonotopy
Descending
Medial olivocochlear efferent
Hearing loss
Deafness

ABSTRACT

Auditory efferent neurons reside in the brain and innervate the sensory hair cells of the cochlea to modulate incoming acoustic signals. Two groups of efferents have been described in mouse and this report will focus on the medial olivocochlear (MOC) system. Electrophysiological data suggest the MOC efferents function in selective listening by differentially attenuating auditory nerve fiber activity in quiet and noisy conditions. Because speech understanding in noise is impaired in age-related hearing loss, we asked whether pathologic changes in input to MOC neurons from higher centers could be involved. The present study investigated the anatomical nature of descending projections from the inferior colliculus (IC) to MOCs in 3-month old mice with normal hearing, and in 6-month old mice with normal hearing (CBA/CaH), early onset progressive hearing loss (DBA/2), and congenital deafness (homozygous Shaker-2). Anterograde tracers were injected into the IC and retrograde tracers into the cochlea. Electron microscopic analysis of double-labelled tissue confirmed direct synaptic contact from the IC onto MOCs in all cohorts. These labelled terminals are indicative of excitatory neurotransmission because they contain round synaptic vesicles, exhibit asymmetric membrane specializations, and are co-labelled with antibodies against VGlut2, a glutamate transporter. 3D reconstructions of the terminal fields indicate that in normal hearing mice, descending projections from the IC are arranged tonotopically with low frequencies projecting laterally and progressively higher frequencies projecting more medially. Along the mediolateral axis, the projections of DBA/2 mice with acquired high frequency hearing loss were shifted medially towards expected higher frequency projecting regions. Shaker-2 mice with congenital deafness had a much broader spatial projection, revealing abnormalities in the topography of connections. These data suggest that loss in precision of IC directed MOC activation could contribute to impaired signal detection in noise.

1. Introduction

The central auditory system is composed of ascending and descending pathways. Olivocochlear (OC) efferents of the brain stem comprise the final stage of these descending pathways as they communicate directly with the sensory receptors of the auditory periphery. In mouse, medial olivocochlear efferents (MOCs) reside bilaterally in the ventral nucleus of the trapezoid body (VNTB) and dorso-medial periolivary nucleus (Brown et al., 2013). MOCs send myelinated axons that terminate on outer hair cells (OHCs). MOC activation effectively decreases cochlear gain, which facilitates signal extraction from background noise, known as 'antimasking'

Abbreviations: ABC, avidin biotin complex; ABR, auditory brainstem response; ANF, auditory nerve fiber; BDA, biotinylated dextran amine; CAP, compound action potential; CM, cochlear microphonic; CNIC, central nucleus of the inferior colliculus; CTB, cholera toxin subunit B; DPOAE, distortion product otoacoustic emission; IC, inferior colliculus; LSO, lateral superior olive; MNTB, medial nucleus of the trapezoid body; MOC, medial olivocochlear; Ni-DAB, nickel intensified diaminobenzidine; NR, no response; OC, olivocochlear; OHC, outer hair cell; VNTB, ventral nucleus of the trapezoid body

* Corresponding author. Garvan Institute of Medical Research, 384 Victoria Street, Darlinghurst, NSW, 2010, Australia.
E-mail address: k.suthakar@student.unsw.edu.au (K. Suthakar).

http://dx.doi.org/10.1016/j.heares.2016.06.014
0378-5955/

(Winslow and Sachs, 1987; Kawase et al., 1993; Kumar and Vanaja, 2004), and promotes protection from acoustic trauma (Rajan, 1988b; a; 1990, 1995; Brown et al., 2003; Maison et al., 2013; Tong et al., 2013; Liberman and Maison, 2014).

Previous anatomical and electrophysiological experiments suggest that the OC system receives descending input from higher auditory centers, including the inferior colliculus (IC; Faye-Lund, 1986; Caicedo and Herbert, 1993; Thompson and Thompson, 1993; Vetter et al., 1993; Mulders and Robertson, 2000a, 2002; Mulders et al., 2010) and auditory cortex (AC; Mulders and Robertson, 2000b; Xiao and Suga, 2002; Perrot et al., 2006; Dragicevic et al., 2015). Electrical stimulation of the IC results in voltage changes reminiscent of both sound and electrical activation of MOC efferents (Mulders and Robertson, 2000a, 2002; Popelar et al., 2002; Groff and Liberman, 2003; Ota et al., 2004; Zhang and Dolan, 2006). Anatomically, descending inputs appear to be arranged in a topographic manner where dorsally placed injections in lower frequency regions label projections more laterally in VNTB, and ventrally placed injections in higher frequency regions label projections progressively more medially (Caicedo and Herbert, 1993; Malmierca et al., 1996). This relationship is consistent with the idea that the MOC filtering operation is optimized by frequency-specific suppression that enables spectral differentiation between signals and noise. In the presence of multiple voice streams, selective spectral filtering directed by descending connections from higher centers would be crucial for speech intelligibility.

Impaired signal extraction in noisy environments is a hallmark feature of age-related hearing loss. We hypothesize that hearing loss may result in an organizational disintegration of descending projections from the IC to auditory efferents. In this study, we have shown that the IC provides direct synaptic input to MOC efferents in hearing, hearing loss, and deafness whose morphology is indicative of excitatory transmission. We have mapped the topographic descending projection from the IC to the region containing MOC efferents, the VNTB, in the normal hearing, adult CBA/CaH mouse. We then investigated this organization of descending IC input in mouse models of early onset hearing loss (DBA/2) and congenitally deaf (Shaker-2) mice.

2. Materials and methods

All methods used for this report followed the guidelines established by the NHMRC and were approved by the Animal Ethics Committee for the Garvan Institute of Medical Research and St. Vincent's Hospital, University of New South Wales.

2.1. Mouse models of hearing, hearing loss and deafness

Three well characterized mouse strains were used in this study. Normal hearing, 3-month old and 6-month old CBA/CaH mice (Zheng et al., 1999) were used as baseline controls from which descending projections from IC to VNTB were investigated. The DBA/2 mouse exhibits early onset hearing loss at around 3 weeks of age due to a mutation in the Cadherin-23 gene (*Cdh23*), which affects the tip links of stereocilia atop hair cells (Willott et al., 1984; Hultcranz and Spangberg, 1997; Johnson et al., 2000; Wang and Manis, 2006). The homozygous Shaker-2 (*sh2/sh2*) mouse exhibits congenital deafness due to a point mutation in the gene, *Myo15*, on chromosome 11, whose expression is limited to the inner ear and pituitary gland (Probst et al., 1998; Liang et al., 1999). Functionally, the shortened stereocilia atop hair cells affect both auditory and vestibular systems producing phenotypic deafness and circling behavior (Beyer et al., 2000; Lee et al., 2003).

2.2. Auditory Brainstem Response (ABR) testing

ABR testing was performed prior to experimentation to verify that the degree of hearing ability in each cohort matched that reported in the published literature. A total of 31 animals were used to compile ABR data from the 3 mouse strains at 1, 3 and 6 months of age (Fig. 1). A subset of this ABR cohort was examined in the course of this study (Table 1). Animals were anaesthetized with ketamine/xylazine (50 mg/kg and 10 mg/kg, respectively) and placed in a double walled, sound attenuated chamber (Sonora Technology Co., Yokohama, Japan), on a battery operated, infrared heat pad. Needle electrodes were inserted into the skin at the vertex and pinna, with a ground reference inserted into the muscle of the hind leg (biceps femoris). Free field click (0.1 ms rectangular pulse, repetition rate of 10/sec) and tone stimuli (4, 8, 16, 24, 32 and 40 kHz; 5 ms duration; 0.5 ms rise-fall) were generated with a signal processor (RZ6; Tucker Davis Technologies [TDT], Alachua, FL) controlled by BioSigRZ software (v5.3; TDT), preamplified (Medusa RA16PA; TDT) and delivered using a magnetic speaker (MF1; TDT). Stimuli were presented at 10 dB decreasing steps from 90 dB SPL to 0 dB SPL. Averaged responses to 512 stimuli presentations were filtered (0.5–3 kHz; notch at 50 Hz), plotted and used to determine threshold.

2.3. Neuronal tract tracing

Discrete deposits of anterograde biotinylated dextran amine (BDA) tracer were made into the central nucleus of the IC (CNIC) to label descending axon projections and their terminals in the VNTB. Injections were guided by *in vivo* electrophysiological recordings of multi-unit responses to sound in awake 3 month (n = 6) or 6 month (n = 2) CBA/CaH mice, or placed stereotaxically in mice with hearing loss (6 month old DBA/2; n = 2) or congenital deafness (6 month old *sh2/sh2*; n = 3). Animals were prepared for awake electrophysiological recordings using published methods to install a head restraint under anaesthesia (Muniak et al., 2012). Briefly, the procedure involved securing the animal in a stereotaxic frame under general anaesthetic (isoflurane; 1.5–2.0% in ~600 cc/min O_2). A midline incision was made on the superior surface of the calvaria for installation of a head post and ground pin. Using a #11 scalpel blade to etch through the bone overlying the inferior colliculus, a

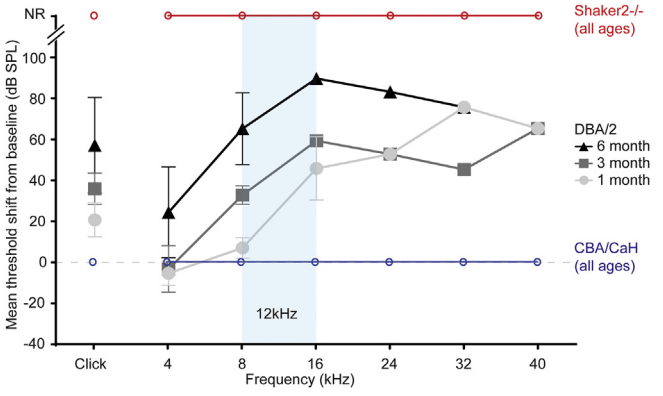

Fig. 1. Auditory Brainstem Response (ABR) thresholds shifts in DBA/2 compared to baseline, normal hearing CBA/CaH mice. At all ages, DBA/2 mice show significant threshold shifts in frequency regions greater than 16 kHz ($p < 0.0001$). One-month old DBA/2 mice start life with normal hearing between 4 and 8 kHz. Threshold shifts for DBA/2 mice are greatest at the 8–16 kHz region, and occur in a progressive manner. Because of the dynamic change in hearing status at this octave band, we targeted this 12 kHz frequency region (blue highlight) for our stereotaxic injections and anatomical analyses. (For interpretation of the references to colour in this figure legend, the reader is referred to the web version of this article.)

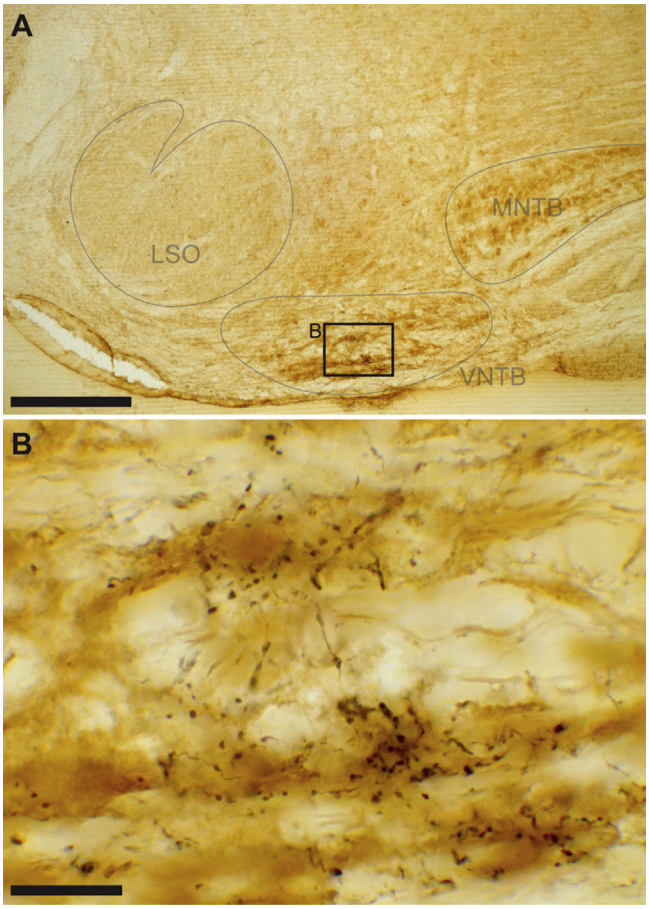

Fig. 2. Discrete injections of BDA were made in the CNIC guided by multi-unit recordings in CBA/CaH mice. The resultant labeling of axonal projections that descended to the VNTB were analyzed for this report. (A) Light micrograph shows the ipsilateral superior olivary complex at low magnification with major subdivisions of the superior olivary complex indicated. LSO – Lateral Superior Olive; MNTB – Medial Nucleus of the Trapezoid Body; VNTB – Ventral Nucleus of the Trapezoid Body. (B) Higher magnification photomicrograph of inset region in (A) revealing descending IC fibers giving rise to bouton endings in VNTB. Boutons as shown in this micrograph were plotted for all cases to determine the spatial distribution of terminal fields. Scale bar equals 250 μm (A) and 25 μm (B).

2 mm^2 craniotomy was made. Bone wax (W31G, Ethicon, Somerville, NJ) was used to cover the craniotomy during all non-experimental periods. Speaker calibration was performed prior to experimentation using a ¼" free field microphone (Type 4939; Bruel and Kjaer, Nærum, Denmark) and preamplifier (Type 2670; Bruel and Kjaer, Nærum, Denmark) positioned within the stereotaxic apparatus to approximate the location of the mouse's contralateral ear. A measuring amplifier (Type 2610; Bruel and Kjaer, Nærum, Denmark) recorded a steady mean 10 dB SPL increase from 4 to 20 kHz, and decrease of a rate about 2.5 dB per 10 kHz from 20 to 100 kHz. Following overnight recovery, the animal was administered a mild sedative (acepromazine; 0.07 mg/kg), and secured in a stereotaxic frame in our sound-attenuated booth. Multiunit recordings were performed using quartz micropipette electrodes (16–20 μm tip diameter; 4–10 MΩ resistance) filled with 10% biotinylated dextran amine tagged with fluorescein (BDA; Cat #D7178, 10 000 MW Life Technologies, Carlsbad, CA) in 0.5 M Tris and 0.15 M KCl. Digitally generated broadband noise stimuli were presented by custom software (*Batlab*; Donald Gans) in a free field arrangement 10 cm away from the contralateral ear, where the speaker was placed 25° off midline. The electrode was advanced into the brain at an angle of 12° using a motorized hydraulic micromanipulator (2650; Kopf Instruments). Sound evoked spike discharges were used to select the injection site in the CNIC. Neuronal responses to tone bursts (4–100 kHz) at 10 dB step decreasing intensities were used to construct multiunit tuning curves, from which best frequency was extrapolated. Following electrophysiological tuning, the cocktail of dyes was iontophoretically injected using a high voltage, constant current source (CS 3; Midgard/Stoelting) set at 5 μA of positive charge, alternating 7 s on and 7 s off for 5–10 min. The electrode was withdrawn 5–10 min after the injection, the craniotomy covered with bone wax, and the animal returned to its cage.

IC injections were guided by electrophysiological recordings or stereotaxic coordinates and made into the region around 12 kHz to allow for comparisons between cohorts. This frequency band is where the DBA/2 mice show the greatest age-related shift in hearing sensitivity (Fig. 1; see also Connelly et al., 2016 in this issue for further discussion). Two additional animals from each cohort also received an injection of cholera toxin subunit B (CTB; 0.5% in 0.5 M Tris buffer, pH 7.6 and 3 M NaCl; List Biological Laboratories, Campbell, CA) through the round window of the cochlea to label olivocochlear efferent cell bodies for electron microscopic analysis of synaptic morphology. Cochlear injections were carried out under general anaesthetic (isoflurane; 1.5–2.0% in ~600 cc/min O_2), along with local administration of an anaesthetic (bupivacaine; 8 mg/kg) and intraperitoneal injection of an analgesic (buprenorphine; 0.1 mg/kg). The cochlea was accessed by a transverse incision behind the right pinna. After removal of the tympanic membrane, incus, and malleus, the bulla was opened to visualize the stapes and stapedial artery. A high temperature, fine tip disposable cautery (Medtronic, North Ryde, NSW, Australia) was used to cauterize the stapedial artery. Upon accessing the round window, small tissue wicks were used to absorb perilymph. A quartz pipette (outside tip diameter of 80–100 μm), attached to a Nanoject II Injector (Drummond Scientific Company, Broomall, PA, USA), was used to slowly inject 5 μl of CTB over a 5-min period. After withdrawing the pipette, the round window was covered with gelfoam, and the wound closed using silk sutures.

After a 10–14 day survival period, animals were deeply anaesthetized with sodium pentobarbitone and perfused intracardially with a prewash of 5 ml of 1% sodium nitrite in 0.1 M phosphate buffered saline followed by 60 ml of 4% paraformaldehyde in 0.1 M phosphate buffer. Heads were postfixed in phosphate buffered 4% paraformaldehyde for 2–3 h (electron microscopic processing) or overnight (brightfield and fluorescence processing). The dissected brain was then embedded in bovine serum albumin hardened with paraformaldehyde and glutaraldehyde, and cut into 50–60 μm thick coronal sections on a vibrating microtome (VT1200S; Leica Systems, Nussloch, FRG).

Immunohistochemical processing was performed on free floating sections using a modified two-day protocol (Ye et al., 2000), which results in anterogradely labelled fibers filled with black reaction product contacting retrogradely labelled efferent cell bodies containing granular, brown reaction product. Rinses were performed thrice within a 15 min window using fresh 0.12 M Tris buffered saline, unless otherwise stated. Tissue was incubated in 1% H_2O_2 for 10 min to remove endogenous peroxidase. Sections were rinsed, permeabilized for 1 h in 0.1–0.5% PhotoFlo (Kodak, Rochester, NY), incubated for 1 h in ABC (Vectastain Elite ABC Kit; Cat# PK-6100; Vector Labs), rinsed and developed using nickel intensified diaminobenzidine (Ni-DAB) enabling visualization of the anterograde tracer BDA. Sections were rinsed again and incubated again in 1% H_2O_2 for 10 min, rinsed and incubated in 1% normal rabbit serum (Cat # S-5000; Vector Laboratories, Burlingame, CA), then incubated overnight at 4 °C on a shaking platform

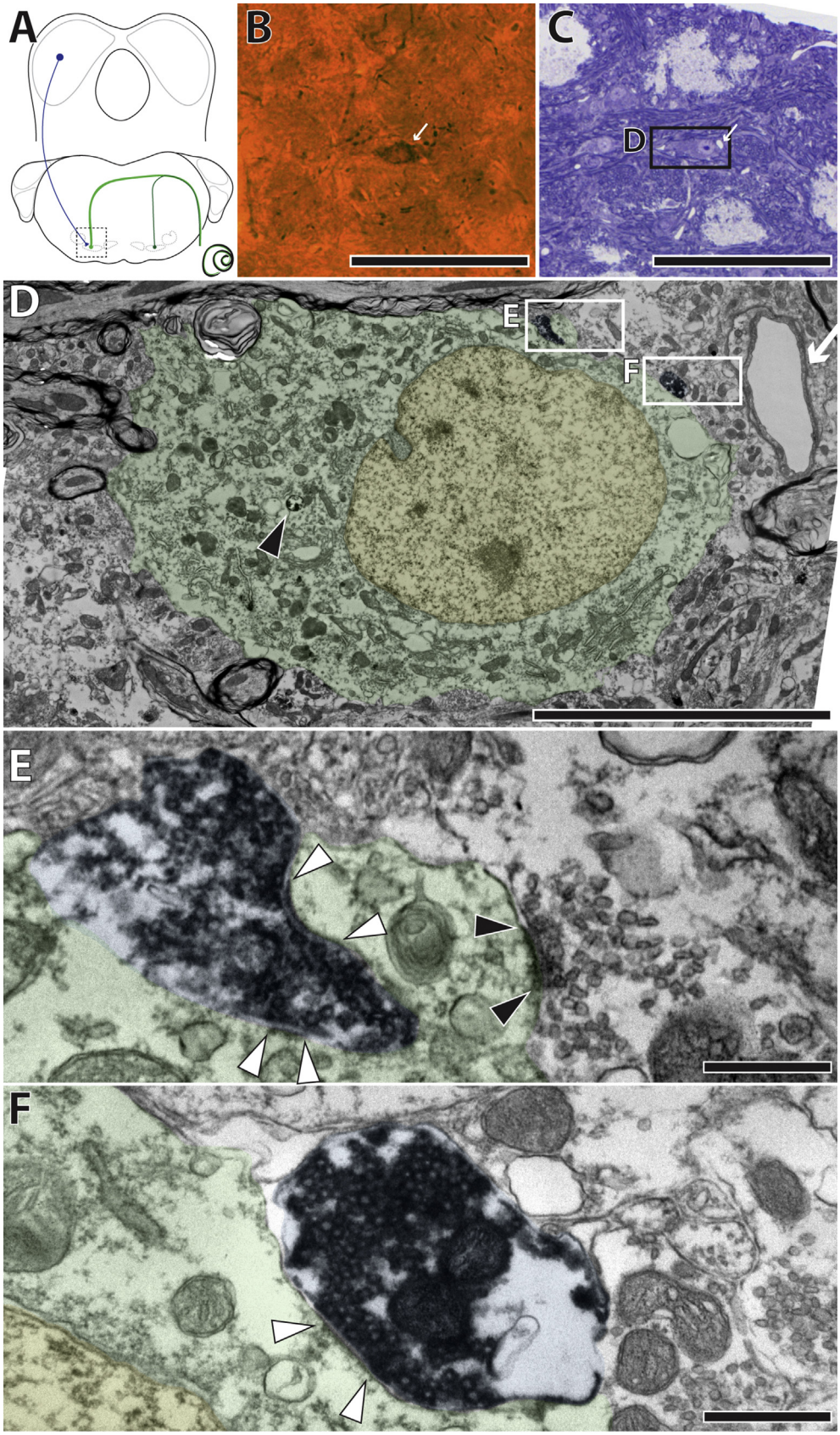

Fig. 3. Electron microscopic evidence of synapses between IC projections and MOC efferents in normal hearing CBA/CaH mice. (A) Schematic illustration of anterograde tracer BDA injected into the left IC (blue) and retrograde tracer CTB injected into the right cochlea (green) of the same animal. Dotted box shows region studied with electron microscopy where anterograde and retrograde labeling converged. (B) Light micrograph of tissue embedded in a BEEM capsule shows BDA labelled axon giving rise to multiple boutons in close proximity to a CTB labelled cell body of a MOC efferent. (C) A light micrograph of the same region of tissue as in (B) in a 250 nm thick, semi-thin section. (D) Electron micrograph of the cell shown in (B) and (C). The cell body has been tinted green and nucleus tinted yellow. Notice the blood vessel located to the right of the cell (white arrow), which is also visible in panel (C). The CTB reaction product is visible in lysosomes (black arrowhead). (E, F) Electron micrographs of labelled terminals synapsing onto a somatic spine (E) and directly onto the soma (F). The density of the reaction product partially obscures the round synaptic vesicles. The prominent postsynaptic membrane thickenings are indicated between the white arrowheads. An unlabelled terminal is also seen synapsing on the somatic spine (E; black arrowheads). Scale bars equal 100 μm (B, C), 10 μm (D), 500 nm (E, F). (For interpretation of the references to colour in this figure legend, the reader is referred to the web version of this article.)

in polyclonal goat anti-CTB primary antibody (1:10,000; Cat# 703, RRID:AB_10013220; List Biological Laboratories). The following day, sections were washed and incubated in biotinylated rabbit anti-goat secondary (1:200; Cat# BA-5000; Vector Labs) for one hour, washed again, incubated in ABC for another hour, and developed using DAB. Some sections were selected for electron microscopic processing (see below), and all other sections were mounted and cover slipped using Permount (Fisher Scientific, Pittsburgh, PA).

To investigate the neurochemical nature of descending IC input in terms of excitatory or inhibitory activation, immunohistochemistry for vesicular glutamate transporter 2 (VGlut2) was performed in animals that received fluorescent BDA injections into the IC, and tissue imaged using a confocal microscope (DMI 6000 SP8; Leica Microsystems, Wetzlar, Germany). Sections were permeabilized in 0.25% Triton X 100 (T8787; Sigma Aldrich, St Louis, MO) for ten minutes, soaked for one hour in 10% normal goat serum with 0.2% Triton X-100, and incubated overnight at 4 °C in rabbit anti-VGlut2 primary antibody (1:1,000; Cat# V2514; RRID:AB_477611; Sigma-Aldrich, St Louis, MO), with 0.2% Triton X-100. The following day, sections were rinsed, and incubated in goat anti-rabbit secondary antibody conjugated to Alexa568 (1:200; Cat# A-11004) for one hour and rinsed a final time before being mounted and cover slipped using Vectashield Hard Set Mounting Medium (H-1400; Vector Labs).

Processing for electron microscopy involved infiltrating the tissue with osmium tetroxide (1% osmic acid in 0.1 M s-Collidine buffer pH 7.4), staining with 1% uranyl acetate, then dehydrating, and embedding in PolyBed 812 (Polysciences, Inc., Warrington, PA) between two sheets of Aclar (Electron Microscopy Sciences, Hatfield, PA). Small regions of interest were cut out from the polymerized Polybed 812 and embedded in a BEEM capsule from which semi thin (250 nm) and ultrathin (70 nm) serial sections were prepared and examined using a transmission electron microscope (H7650; Hitachi, Tokyo, Japan).

2.4. Quantitative analysis

ABR data were uploaded to a custom built web based analysis program (*openabr.org*, Samuel Kirkpatrick), where computer-controlled thresholds, defined as the level of sound presentation (dB SPL) required for peak amplitude signals to be greater than 4 standard deviations above the baseline noise (Bogaerts et al., 2009), were recorded. Thresholds were then analyzed using 2-way ANOVA and Sidak's multiple comparison test using Prism (Graphpad, La Jolla, CA).

The location of each labelled terminal was plotted using Neurolucida software (Microbrightfield, Essex, VT, USA) attached to light microscope (Nikon, Eclipse E600) controlled via a motorized stage (LEP, Ludl Electronic Products, Hawthorne, NY). Anatomical landmarks including the midline, inferior cerebellar peduncle and nuclei of the superior olivary complex were traced in each section to assist in serial section orientation and 3D reconstruction. Data were imported and processed in MATLAB (Mathworks, Natick, MA). Due to variations in sectioning orientation and to account for tissue shrinkage between animals, the raw data were normalized per case so the location of individual labelled terminal was represented as a proportion of the distance between the midline and peduncle where the peduncle to midline distance was defined as 100%. The mean peduncle distance across all cases was then used to normalize across cases. Within cases, the terminal bouton density was calculated by section, where 100 bins were drawn from the 100% distance from midline to peduncle. The number of terminals in each bin was then divided by the total number of terminals in that case. Statistical analyses of terminal data were performed on normalized section means grouped by case. This approach allowed us to analyze the region of greatest terminal density, and utilized the standard deviations of each section as a measure of degree of mediolateral spread (within cases) along the rostrocaudal axis (between cases). One-way ANOVA and the Brown-Forsythe test were used to analyze normalized section means and standard deviation data in Prism (Graphpad, La Jolla, CA).

3. Results

3.1. Strategy for investigating descending IC projections in hearing loss

The goal of this project was to analyze synapse morphology and quantify the spatial distribution and topographic projections in mice with respect to hearing status. Thus, we created our experimental cohorts on the basis of functional hearing of strains verified against previous reports using ABR testing. A 2-way ANOVA showed significant differences in hearing thresholds across frequencies ($p < 0.0001$) and cohorts ($p < 0.0001$) with a significant interaction ($p < 0.0001$). Sidak's multiple comparison test, however, showed no significant change in thresholds between CBA/CaH mice at any of the frequencies tested at 1, 3 or 6 months of age. Thus, CBA/CaH mice of all ages were pooled, and used as our baseline standard (Fig. 1). Homozygous Shaker-2 mice were verified to be congenitally deaf, as they did not exhibit sound evoked neural activity at any age. Because the *sh2/sh2* mouse receives no auditory input at any age, we reasoned that reorganization of descending terminals would be consistent across the entire frequency spectrum. They were called unresponsive and used as the “ceiling” to our plots.

The DBA/2 animals emerged as the best subjects to investigate the effects of hearing loss on descending projections because they have hearing at birth and experience progressive threshold elevation starting at high frequencies and spreading to lower frequencies as the animal ages (Fig. 1). Thresholds of CBA/CaH mice at all ages were grouped, and means at each frequency were used to compare threshold shifts in DBA/2 mice at 1, 3, and 6 months of age. This threshold shift occurred in the 8–16 kHz range in an age-graded progressive fashion. Therefore, projections of the 12 kHz frequency region were targeted by stereotaxic injections in 6 month old DBA/2 and *sh2/sh2* mice in order to assess changes related to hearing loss. The 12 kHz frequency region was also targeted in aged CBA/CaH mice to verify that observed changes were attributable to hearing status rather than age alone.

3.2. Synaptic input from the inferior colliculus projections upon MOC efferents in hearing, hearing loss, and deaf animals

Injections of the anterograde tracer, BDA, were made into the CNIC. Immunohistochemical processing allowed for visualization of the injection site in the CNIC from which descending projections coursed ventrally through the lateral lemniscus and arborized in and about the ipsilateral VNTB (Fig. 2A) to create a field of *en passant* and terminal boutons (Fig. 2B). Boutons were defined as swellings with a diameter at least two times greater than their parent axons. *En passant* and terminal boutons could be clearly observed by focusing up and down through the tissue section, and those that fit the above criterion were plotted using *Neurolucida* software.

In all mice that received combined injections of BDA in the IC and CTB in the cochlea (Fig. 3A), light microscopic analyses revealed anterogradely labelled IC projections in close apposition with retrogradely labelled MOC efferents (Fig. 3B). Labelled cells of interest were identified in subsequent 250 nm thick, semi-thin

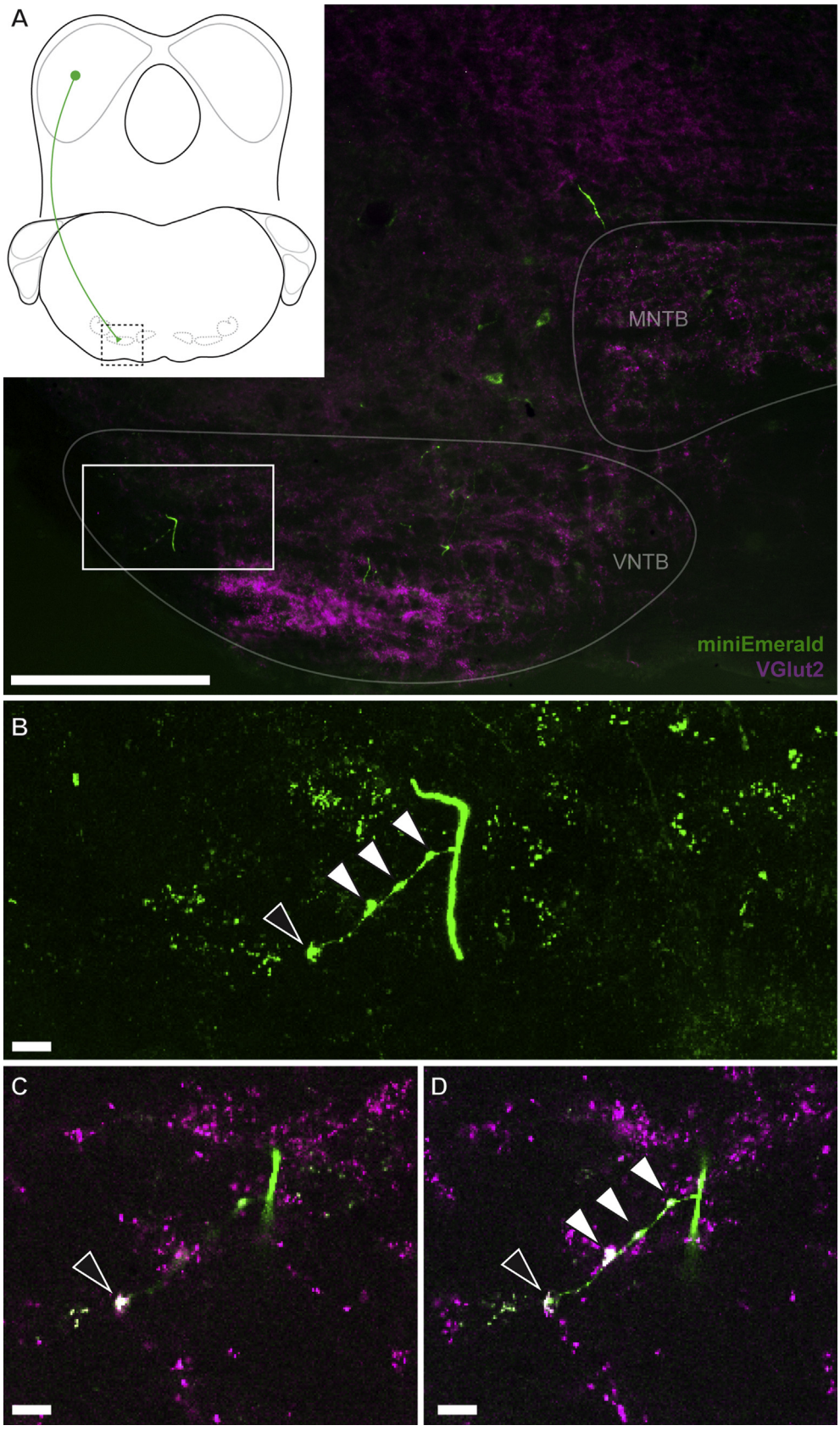

Fig. 4. VGlut2 immunostaining of descending projections from IC to MOCs. (A) Photomicrograph of superior olivary complex region in a CBA/CaH mouse that received an injection of BDA-miniEmerald (green) into the IC followed by immunostaining for VGlut2 (magenta). A schematic drawing in upper left indicates the location of the region of interest with a dotted box. (B) Higher magnification of a confocal maximum projection z stack (boxed region in A) showing a descending fiber giving rise to boutons (arrowheads). (C, D) Confocal images of the same region at different z planes showing co-localization of BDA and VGlut2 (white) in boutons, indicated by the arrowheads. Scale bars equal 250 μm (A), 10 μm (B–D). (For interpretation of the references to colour in this figure legend, the reader is referred to the web version of this article.)

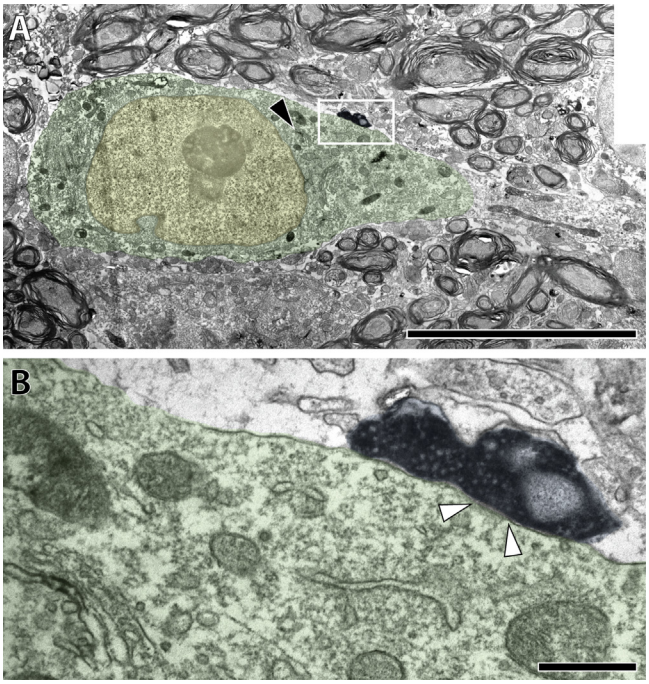

Fig. 5. Representative electron micrographs of synapse between a descending IC axon terminal and a MOC efferent neuron in a 6-month-old DBA/2 mouse. (A) The cell body of the MOC efferent has been tinted green and the nucleus colored yellow. An anterogradely labelled terminal is seen contacting the soma (box) and CTB reaction product is indicated by the black arrowhead. (B) Higher magnification electron micrograph of the axosomatic synapse formed between the labelled terminal and MOC efferent cell body. The postsynaptic density is indicated between the white arrowheads. The synapse appears asymmetric and the vesicles round, indicative of excitatory neurotransmission. Qualitatively, no change in synaptic morphology appeared to accompany hearing loss. Scale bars equal 10 μm (A), 500 nm (B). (For interpretation of the references to colour in this figure legend, the reader is referred to the web version of this article.)

sections using nearby landmarks such as blood vessels (Fig. 3C and D). In normal hearing 3-month old CBA/CaH mice, terminals arising from descending IC projections were found to synapse directly on MOC efferent cell bodies (Fig. 3D–F). In our tissue, the cytosolic CTB reaction product was clearly visualized either packaged into the lysosomes (Fig. 3D, black arrowhead) or occasionally observed as electron dense material coupled with the nuclear envelope, endoplasmic reticulum, and Golgi apparatus. Retrogradely labelled MOC neurons showed characteristic ultrastructural properties including the concentric arrangement of Golgi apparatus, arrays of rough endoplasmic reticulum, and other organelles around the nucleus (Benson and Brown, 2006). The nuclear envelope was highly invaginated and contained a conspicuous, centrally placed nucleolus. Large dendrites could be distinguished from the somata via the parallel arrangement of organelles. Anterogradely labelled terminals contained round synaptic vesicles and exhibited asymmetric postsynaptic densities, although the density of the reaction product interfered with attempts at quantifying vesicle size and shape. Consequently, immunohistochemical processing was utilized to buttress the presumed excitatory nature of descending projections. The primary excitatory neurotransmitter in the IC is glutamate (Saint Marie, 1996; Kelly and Caspary, 2005), and the VNTB is known to contain glutamatergic terminals that can be labelled using VGlut2. Analysis of double-labelled fluorescent tissue using confocal microscopy indicated that descending IC terminals in VNTB co-localize with VGlut2 (Fig. 4).

Electron microscopic analysis confirmed that synapses of descending projections of the IC onto retrogradely labelled MOC efferents were present in 6-month old DBA/2 mice (Fig. 5) and 6-month old *sh2/sh2* mice (Fig. 6). Analogous to the methods employed for normal hearing mice, retrogradely labelled MOC efferents appearing to receive anterogradely labelled descending projections from the IC were first identified using light microscopy. Labelled terminals in DBA/2 mice with hearing loss appeared qualitatively similar to those observed in normal hearing animals,

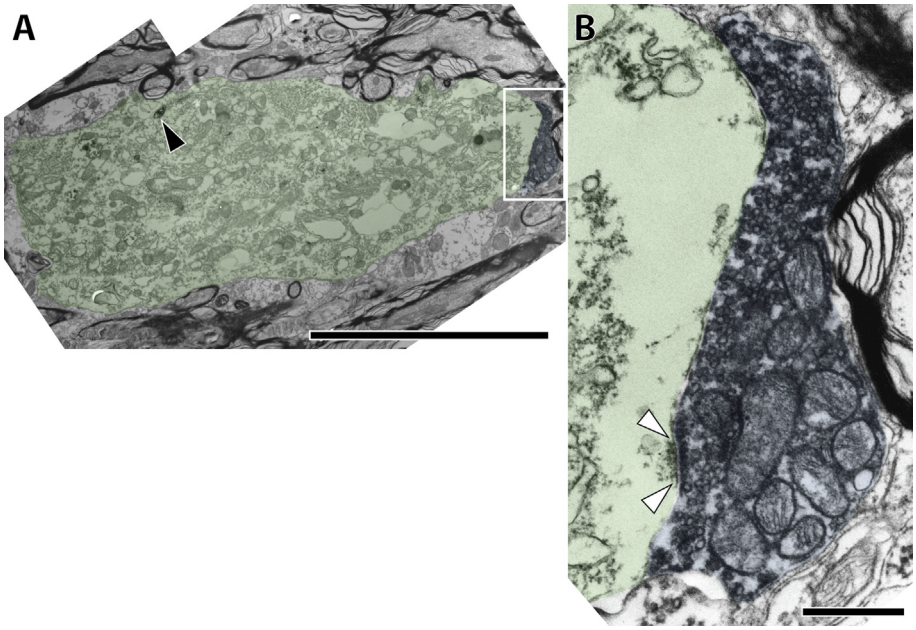

Fig. 6. Representative electron micrograph of synapse between an IC terminal and a MOC efferent cell body in a 6 month old deaf Shaker2 mouse. (A) A section through this MOC neuron (tinted green) shows a labelled terminal (tinted blue) making contact. Its nucleus is not visible in this section, but CTB reaction product is visible (black arrowhead). (B) Higher magnification electron micrograph shows the axosomatic synapse with better details. These terminals exhibit round synaptic vesicles and asymmetric postsynaptic densities (indicated by white arrowheads). Scale bars equal 10 μm (A), 500 nm (B). (For interpretation of the references to colour in this figure legend, the reader is referred to the web version of this article.)

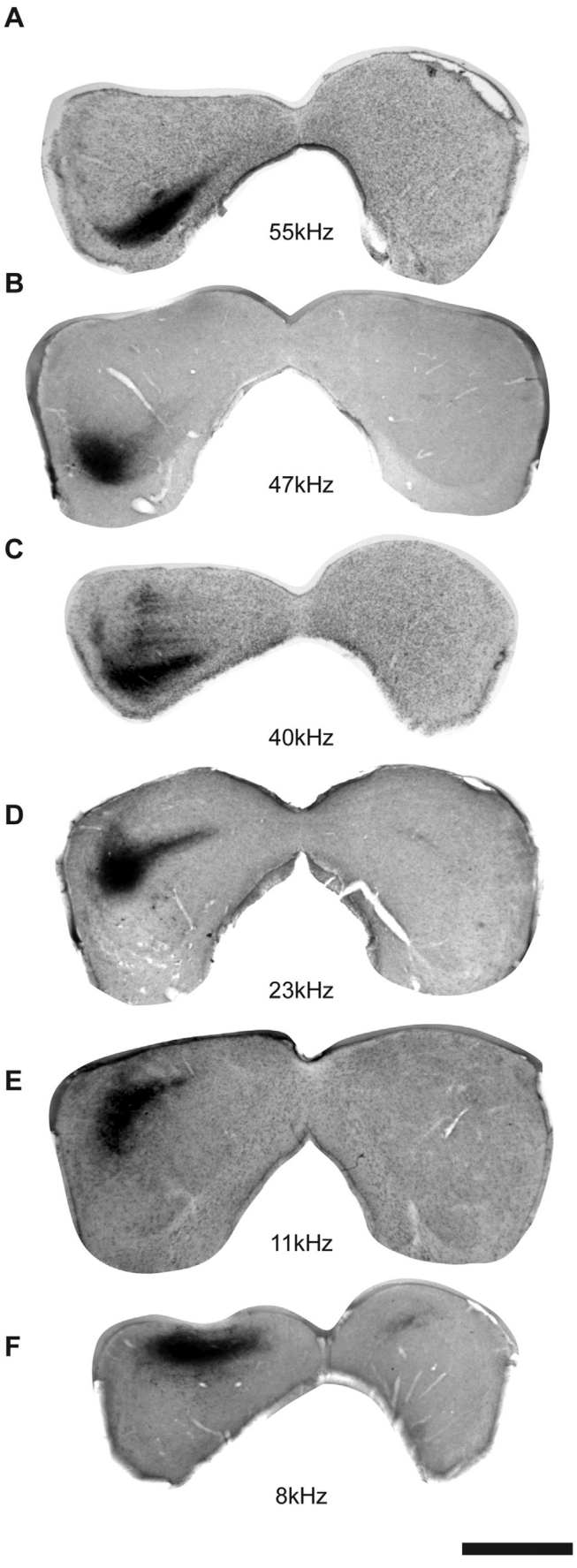

possessing round synaptic vesicles and asymmetric postsynaptic densities (Fig. 5B). Hearing loss did not appear to affect synaptic structure in terms of synaptic vesicle size and shape or postsynaptic density length and thickness. Despite a complete lack of sound driven activity in congenitally deaf *sh2/sh2* mice, synapses of labelled IC projections appeared qualitatively similar to those of CBA/CaH and DBA/2 mice. There appeared to be a normal complement of round synaptic vesicles and asymmetric postsynaptic densities.

3.3. Frequency organization of descending input in normal hearing animals

BDA injections were made in normal hearing, 3-month old CBA/CaH mice, at best frequencies of 55, 47, 40, 23, 11 and 8 kHz (Fig. 7). There is a systematic relationship between recorded frequency and location of the injection site in the CNIC where characteristic frequency of neurons in the central nucleus, going from high to low, progresses in a ventral-to-dorsal fashion. This tonotopic organization has been observed in the CNIC of other mammals (Rose et al., 1963; Merzenich and Reid, 1974; Roth et al., 1978) and gave us confidence that we could analyze the distribution of terminals in the VNTB with respect to characteristic frequency recorded in the IC.

The distribution of labelled terminals from these injections was plotted in 3D in the ipsilateral VNTB using *Neurolucida* software. In each case, terminals were distributed along the mediolateral and rostrocaudal aspects of the VNTB. Even in raw plots, where terminal density is not taken into account, mediolateral variation was evident with respect to frequency of injection site: descending terminals from higher frequency regions were located in medial VNTB regions, whereas lower frequency injections produced terminals distributed more laterally (Fig. 8A–F).

Heat maps of normalized data allowed investigation of two aspects not clearly evident in the raw plots: firstly, the density of boutons in the z dimension within each case (i.e., the point of greatest density along the mediolateral axis per section), and, secondly, the normalized mediolateral position of boutons between cases. Heat maps also illustrate the within case bouton density along the rostrocaudal aspects with respect to frequency of injection site. Bouton density reflects the proportion of total boutons counted for that case where yellows represent greater bouton density, and reds represent lesser bouton density. When bouton density is assessed, a clear trend is visible in both medial-lateral and rostral-caudal axes. Higher frequencies project more medially and lower frequencies project more laterally. A 1-way ANOVA showed that the mean mediolateral location varied significantly with frequency ($p < 0.0001$, Fig. 8G–L).

In all cases, bouton density is greater in rostral sections compared to caudal sections (Fig. 8G–L). The spatial relationship of frequency to terminal distribution was quantified by determining the normalized location of each terminal (mean and standard deviation) for each section and plotting these data on a case by case basis (Fig. 8M–R). No clear trend was observed between injection size (measured using reconstructed volume in μm^3; Table 1), total bouton count, or bouton spread. The Brown-Forsythe test indicated that no significant variance was observed in standard deviations of

Fig. 7. Photomicrographs of CNIC injection sites in individual CBA/CaH mice. The anterograde tracer, BDA, was iontophoretically injected in order to label descending projections to the VNTB, and visualized by reacting tissue with nickel intensified diaminobenzidine, which formed a dark reaction product. Tuning curves constructed from data recorded at each injection site identified the frequency regions as 55 kHz, 47 kHz, 40 kHz, 23 kHz, 11 kHz, and 8 kHz. The subsequent projections of these injections are shown in Fig. 8. Scale bar equals 1 mm (A–F).

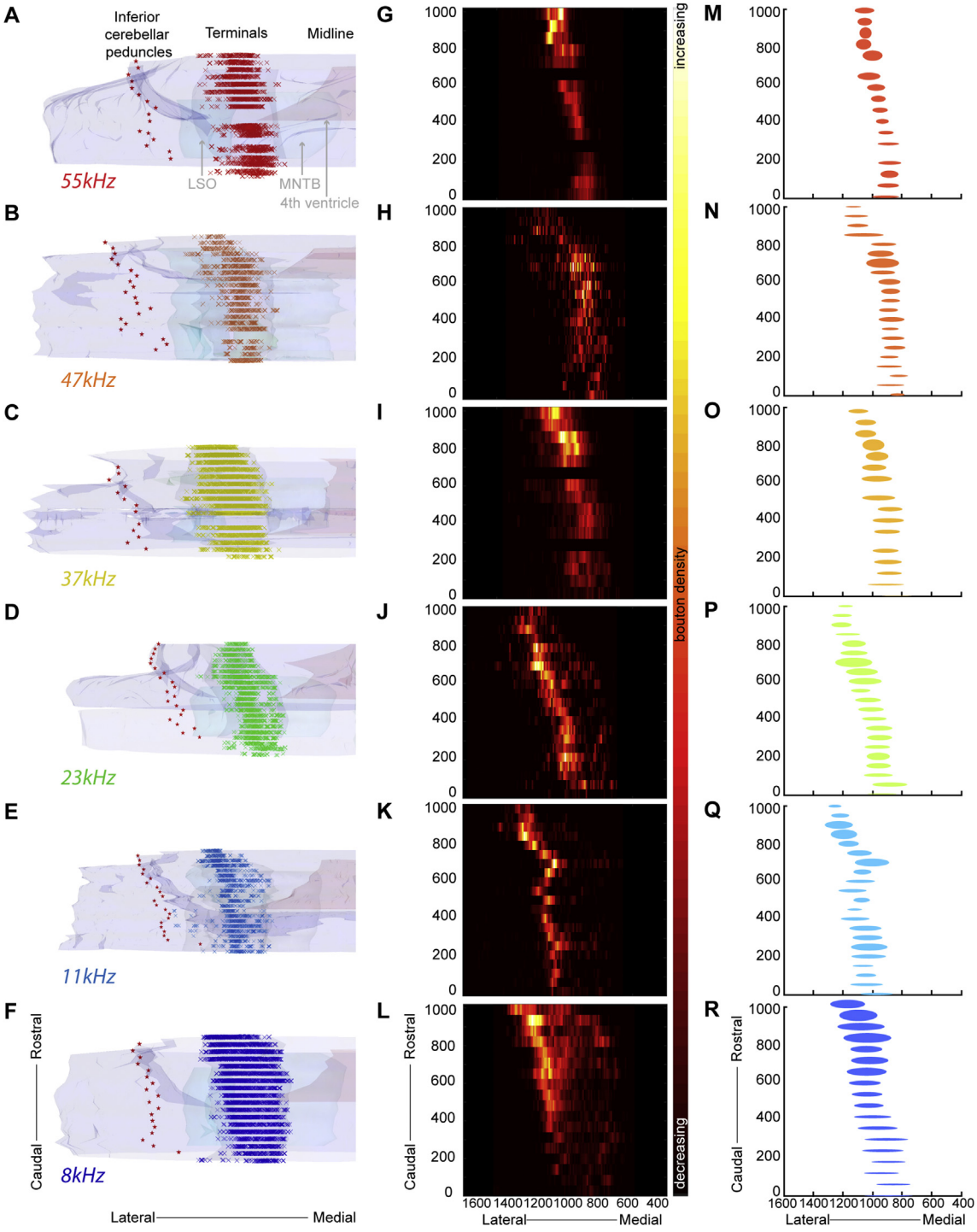

Fig. 8. Frequency organization of the descending terminal fields in individual CBA/CaH mice (by rows). Plots are from injections made into different frequency regions in the CNIC: 55 kHz, 47 kHz, 40 kHz, 23 kHz, 11 kHz, and 8 kHz. (A–F) 3-dimensional renderings of boutons in VNTB viewed from a dorsal aspect of the brain through the superior olivary complex illustrating the spatial distribution of boutons (colored Xs) along the mediolateral and rostrocaudal aspect (unnormalized data). Anatomical landmarks are indicated with red stars (inferior cerebellar peduncle), red shading (fourth ventricle), cyan shading (lateral superior olive [LSO]), and grey shading (medial nucleus of the trapezoid body [MNTB]). (G–L) Heat maps of normalized data illustrate the density of boutons along mediolateral and rostrocaudal aspects. Yellows represent greater bouton density and reds represent lesser bouton density in the z dimension. A clear trend is evident when bouton distribution is considered; higher frequencies project more medially and lower frequencies project more laterally. In every case, bouton density is greater in rostral sections compared to caudal sections. (M–R) Plots of each case showing relative bouton density (ellipse height) and mean ± SD (ellipse center and length, respectively). Section based standard deviations did not vary significantly between cases, suggesting the mediolateral terminal spread across the rostrocaudal axis was consistent between cases. A one way ANOVA performed on section means showed that there was significant differences in mediolateral location ($p < 0.0001$), indicating that the mean terminal location varied with frequency, consistent with the tonotopic heat maps.

Table 1
Injection and bouton data for each case by cohort. Estimated injection volumes were calculated using tracings of the injection site. No clear relationship could be identified between injection parameters (e.g. tip diameter, injection/rest time, estimated injection volume) and total boutons plotted. Asterisks (*) indicate that some sections were processed for electron microscopic analysis and were not plotted.

Hearing status	Strain	Age	Case	Character-istic frequency (kHz)	dB (Attenuation)	Resistance (MΩ)	Tip diameter (μm)	Injection/ Rest (mins)	Section thickness (μm)	Sections plotted	Total distance plotted (μm)	Estimated injection volume (mm^3)	Total boutons plotted
Normal Hearing	CBA/ CaH	3 month	AM474	55	65	10	18	5/5	60	16*	1080	0.16	12,108
			AM192	47	79	7	16	10/5	50	21	1050	0.12	1672
			AM473	37	73	10	18	5/5	60	16*	1020	0.11	16,535
			M319	23	90	5	20	10/10	50	21	1050	0.15	4374
			M355	11	64	6	18	5/5	50	21	1050	0.09	3899
			AM616	8	69	4	20	5/5	60	18	1020	0.25	14,279
		6 month	AM214	14	93	6	16	7/5	50	21	1050	0.06	2084
			AM215	13	103	7	16	7/5	50	21	1050	0.25	7070
Early onset HL	DBA/ 2		AM286	n/a	n/a	–	20	5/5	50	21	1050	0.12	3606
			AM287	n/a	n/a	–	20	7/5	50	21	1050	0.14	7080
Congenitally deaf	sh2/ sh2		AM235	n/a	n/a	–	20	5/5	50	21	1050	0.13	2716
			AM306	n/a	n/a	–	20	7/4	50	21	1050	0.13	4935
			AM317	n/a	n/a	–	20	6/5	50	21	1050	0.15	3951

terminals between cases, suggesting that the overall spread of terminal endings in the VNTB is relatively consistent across all frequencies investigated. Taken together, these results suggest that while the location of the greatest terminal density shifts as a function of characteristic frequency, the relative distribution of terminals along the rostrocaudal and mediolateral axes remained constant.

3.4. Descending input in normal hearing animals

To verify that potential changes to descending projections to MOC efferents from the IC are representative of hearing loss rather than senescence, 6-month-old normal hearing CBA/CaH mice were subjected to the same injection parameters in the 12 kHz region. The recorded best frequencies from these injection sites were 13 kHz and 14 kHz (Fig. 9A–B). 6-month mice showed no significant difference to 3-month mice in terms of terminal spread across the mediolateral axis, measured by standard deviation around the section mean, suggesting that the mediolateral spread of terminals in VNTB is unaffected by age (Fig. 10). In both cases, as expected, the mean terminal location was slightly medial to the 11 kHz range, however, this shift was not statistically significant.

3.5. Descending input in 6-month old mice with hearing loss

The spatial organization of descending projections in mice with hearing loss was investigated using injections directed into the 12 kHz region of the CNIC (Fig. 9C–D). This location was determined using stereotaxic coordinates calculated from recovered injection sites at the 11 kHz region of an adult normal hearing CBA/CaH mouse (Fig. 7E) and the 13 kHz and 14 kHz regions of aged normal hearing CBA/CaH mice (Fig. 9A–B). In this way, terminal location data are compared to the normal hearing 11 kHz case (Fig. 8E,K, Q). Terminals of descending projections were present along the entire rostrocaudal and mediolateral aspects of the VNTB (Fig. 11A–B). Terminal density as revealed by heat maps was greatest in rostral sections, and no significant difference was observed in variance indicating a rostro-lateral migration similar to that observed in normal hearing animals (Fig. 11C–D). The mediolateral location of boutons per section in the hearing loss cases showed significant medial shifting compared to the 11 kHz normal hearing case (Fig. 11E–F; $p < 0.001$) but did not differ significantly in terms of mediolateral spread (i.e. SD around the section mean).

3.6. Descending input in 6-month old deaf mice

When comparing injections in the 12 kHz region of the IC between deaf *sh2/sh2* cases (Fig. 9C–E), labelled projections appeared less consistent and orderly than all other cohorts (Fig. 12A–C). We used data from the 3-month hearing CBA/CaH case (11 kHz) for comparison. Qualitative plots of boutons in both the rostrocaudal and mediolateral dimensions showed varying degrees of patchiness (Fig. 12A–C). Heat maps accounting for terminal density illustrated this patchiness, and variability of terminal density on the rostrocaudal axis (Fig. 12D–F). Unlike the hearing loss cases, however, terminals in deaf cases were not generally shifted compared to the normal hearing 11 kHz CBA/CaH. They did, however, exhibit significantly greater mediolateral spread (Fig. 12G–I). The SDs around the section mean in all deaf cases showed significantly greater variance ($p < 0.05$), indicating that the mediolateral location of terminals across the rostrocaudal dimension was much broader on average.

4. Discussion

The tonotopic organization of the auditory system emphasizes the crucial role of frequency discrimination that underlies our ability to separate one sound from another. We confirmed the topographic descending projections from the CNIC to MOC efferent neurons in the VNTB in normal hearing animals (Caicedo and Herbert, 1993; Malmierca et al., 1996). We extended knowledge of these projections by documenting synapses between these projections and MOC neurons, immunostaining these projections for the glutamate transporter VGlut2, and revealing the terminal fields in three-dimensions using computer-aided microscopy. Finally, we show that the systematic nature of these projections become less precise in a manner proportional to severity of hearing loss, but not age.

4.1. Role of descending projections

Higher auditory nuclei are able to influence afferent input at the earliest stage of the auditory system via descending pathways, which culminate at the auditory efferents (Mulders and Robertson, 2000a; b; Malmierca and Ryugo, 2010, 2011). Auditory cortex projects in a topographic way to VNTB, reiterating the tonotopic projections of the IC (Feliciano et al., 1995). MOC efferents shift the dynamic range of auditory nerve fiber (ANF) responses via their inhibitory effects on OHCs. Individual MOC fibers are relatively sharply tuned, with slightly wider tips relative to frequency-

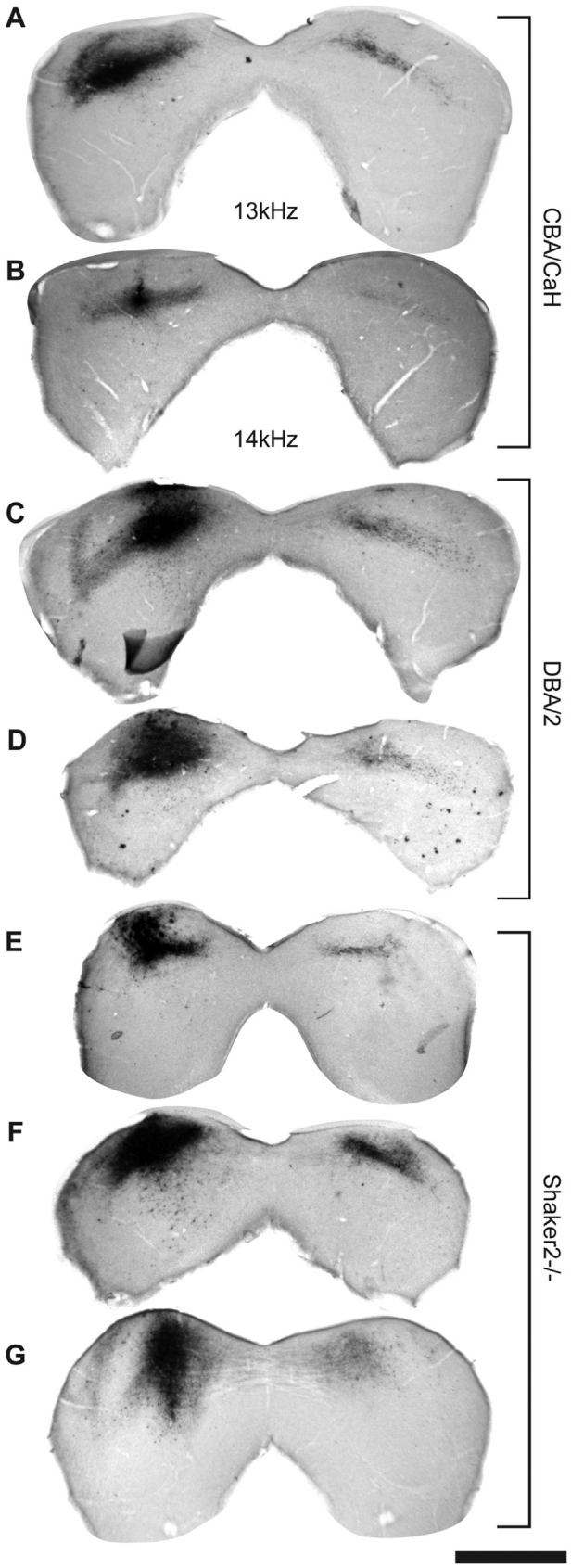

Fig. 9. Injection sites in the IC of 6-month old mice with normal hearing, hearing loss, or congenital deafness. (A–B) Electrophysiologically directed injections in normal hearing 6-month old CBA/CaH mice were made at 13 kHz (A) and 14 kHz (B). Discrete placement of neuronal tracer into the approximate 12 kHz region was directed by stereotaxic coordinates derived from reconstructions of frequency laminae of hearing mice. (A–B) Injections into DBA/2 mice and (C–E) injections into deaf Shaker-2 mice. These injection sites correspond in a location resembling that of 11 kHz in normal hearing mice (Fig. 7B).

matched ANFs (Robertson, 1984; Liberman and Brown, 1986), and exhibit lower activation thresholds in noise, compared to quiet (Winslow and Sachs, 1987, 1988; Liberman, 1988). MOC activation can be evoked by broadband noise or tones where the greatest effects on ANFs occur when matched in frequency (Liberman, 1989). These observations are consistent with the tonotopic projections of olivocochlear efferents to the hair cell receptors (Guinan et al., 1984; Robertson, 1984; Liberman and Brown, 1986). The frequency selectivity exhibited by MOCs, especially in the presence of noise, facilitates operations affecting stimulus selection such as filtering and attention (Ryugo, 2010). Given the increased variability of IC projections to the MOC efferents in hearing loss, it seems likely that these less precise spatial terminations could impair the discrimination between acoustic streams dependent on spectral differences.

Acoustic stream segregation in noise also utilizes sound localization cues (Bregman, 1994; Middlebrooks and Onsan, 2012; David et al., 2015). It is noteworthy that there is OC enhancement of sound localization in the presence of background noise (May et al., 2004). Lesions that involve MOC connections with the inner ear result in an inability of ferrets to compensate for unilateral ear plugging during a sound localization task. Normal localization skill returns following removal of the ear plug (Irving et al., 2011). These results imply that MOC efferents are involved in adaptive behavior that compensates for unilateral hearing loss. A related study in humans reported that the ability to locate a sound source co-varied with the strength of MOC reflex suppression (Andeol et al., 2011). Collectively, these observations support the notion that OC activity has a role in sound localization in the presence of noise and a disruption of IC projections to the MOC could affect this process. By extrapolation, such deterioration would affect speech understanding in noise, a major complaint associated with hearing loss.

4.2. MOC efferents receive direct, excitatory synaptic input from the IC

Electrical stimulation of the IC results in tonotopic attenuation of the incoming afferent signal. CNIC activation results in a decrease in compound action potential (CAP; measure of gross ANF activation), an increase in cochlear microphonic (CM; measure of OHC activity), and a suppression of distortion product otoacoustic emission (DPOAEs; Mulders and Robertson, 2000a, 2002; Popelar et al., 2002; Groff and Liberman, 2003; Ota et al., 2004). These effects were retained after sectioning of the middle ear muscles (Scates et al., 1999), but disappeared after sectioning of the olivocochlear bundle (Zhang and Dolan, 2006), directly implicating MOC efferent involvement.

IC shocks evoke MOC-like effects, so it follows that descending inputs onto MOC efferents would be excitatory. VNTB is a heterogeneous nucleus, both in terms of constituent cells and axonal input. VNTB is known to house inhibitory glycinergic and GABAergic (Helfert et al., 1989; Vetter et al., 1991) cells in addition to the cholinergic MOC efferents (Yao and Godfrey, 1995, 1998, 1997). Projections into the VNTB are similarly heterogeneous, with terminals identified as glutamatergic (Billups, 2005; Blaesse et al., 2005), noradrenergic (Wang and Robertson, 1997), and serotonergic (Woods and Azeredo, 1999).

Glutamate is the primary excitatory neurotransmitter utilized in the IC (Adams and Wenthold, 1979), and terminals in the VNTB are

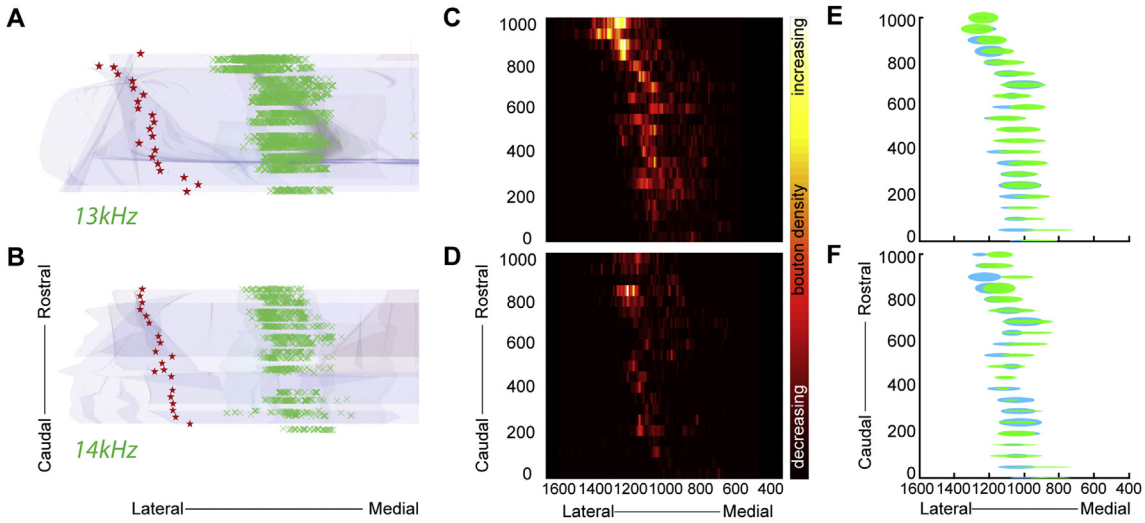

Fig. 10. Frequency organization of the descending terminal fields in individual 6-month-old CBA/CaH mice. (A–B) 3-dimensional renderings of boutons (green crosses) in VNTB viewed from the dorsal aspect showing the terminal distribution through the superior olivary complex. (C–D) Heat maps of normalized data from each case show bouton density with respect to spread along the mediolateral and rostrocaudal axes. (E–F) Plots of each case (green) show relative bouton density (ellipse height) and mean ± SD (ellipse center and length, respectively), with data from the 11 kHz CBA/CaH (blue) plotted for reference.

strongly labelled for VGlut2 but not VGlut1 (Billups, 2005). Using a combination of electron and confocal microscopy we were able to confirm that boutons from IC cells synapse directly onto MOC efferents in normal hearing mice. These labelled terminals exhibit round synaptic vesicles and asymmetric postsynaptic densities that are highly suggestive of excitatory neurotransmission. Co-localization of VGlut2 is consistent with the idea that these terminals are excitatory in nature.

4.3. Direct descending tonotopic input from the IC to MOCs

The tonotopic gradient of the ascending auditory system appears to be mirrored by the descending pathway. In normal hearing animals, descending projections from the auditory cortex (Feliciano et al., 1995) and IC to the VNTB (Caicedo and Herbert, 1993; Malmierca et al., 1996) demonstrate a tonotopic gradient where high frequency terminals project medially and low frequency projections project laterally. Retrograde tracing experiments suggest that MOC efferent cell bodies in VNTB are topographically organized with respect to the location of their peripheral projections in the cochlea (Guinan et al., 1983, 1984; Robertson et al., 1987). Additionally, dye injections confirm that the peripheral termination of electrophysiologically tuned MOC efferents matches the cochlear place of auditory nerve fibers mapped by characteristic frequency (Robertson, 1984; Liberman and Brown, 1986; Brown, 1989, 2014).

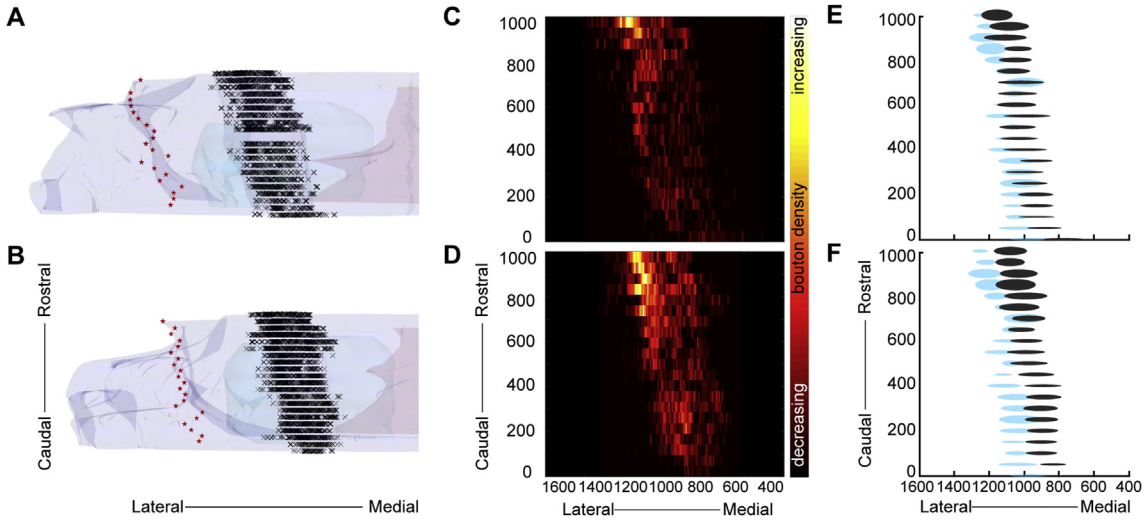

Fig. 11. Frequency organization of the descending terminal fields in individual 6-month-old DBA/2 mice. (A–B) 3-dimensional renderings of boutons (black crosses) in VNTB viewed from a dorsal aspect of the brain show their distribution through the superior olivary complex. (C–D) Heat maps of normalized data from each case show bouton density with respect to spread along the mediolateral and rostrocaudal axes. (E–F) Plots of each case (black) show relative bouton density (ellipse height) and mean ± SD (ellipse center and length, respectively), with data from the 11 kHz CBA/CaH (blue) plotted for reference. In both cases of hearing loss, the normalized distribution of descending terminals was shifted medially compared to the normal hearing CBA/CaH at 11 kHz ($p \leq 0.01$). There was, however, no significant difference in variance between the two DBA/2 cases, or compared to the normal hearing CBA/CaH, suggesting that the spread of boutons along the mediolateral aspect remained consistent in hearing loss and was comparable to that seen in normal hearing.

4.4. Decoding the contribution of descending pathways

Our observations on descending projections to MOC efferents merit some additional comments. While MOC efferent activity appears to be involved in extracting signals from noise, the mechanisms for distinguishing signal from noise remains to be determined. A number of characteristics common to both the IC and MOCs imply that descending projections may provide multimodal contextual cues by assigning relevance and importance to some sounds over others. Within the context of hearing, the IC is a region where auditory and non-auditory inputs converge. Increases in MOC activity have been shown to occur with tasks involving these same non-auditory systems. Consequently, the IC represents a fitting candidate to provide the accessory information used to fine tune MOC gain control.

The addition of cross-modal attentional cues can influence auditory performance. Visual discrimination and attention tasks shift auditory evoked potentials (Oatman, 1971, 1976; Oatman and Anderson, 1977; Lukas, 1981), compound action potentials (CAPs), and cochlear microphonics (CMs) in a manner analogous to MOC activation (Delano et al., 2007). Furthermore, the magnitude of these cochlear effects is correlated to the level of attentional demand, and the time course is linked to the onset of attention (Delano et al., 2007).

The IC receives input from the visual system and is implicated in complex attentional processes related to anticipatory behavioural performance. IC cells receive direct retinal innervation (Morin and Studholme, 2014), respond to light stimulation (Syka and Radilweiss, 1973; Tawil et al., 1983), and use eye position information such as saccades (Groh et al., 2001; Porter et al., 2007) to integrate auditory and visual information. In the CNIC, single unit discharge rates in response to sound are increased during reaction time tasks that use visually alerting stimuli (Ryan and Miller, 1977; Ryan et al., 1984). With respect to saccadic performance, this integration appeared to be reflexive as the maintenance of fixation was not required for significant IC activation (Porter et al., 2007). However, when saccadic performance was paired with an anticipatory reward, some IC cells would exhibit a stronger response (Metzger et al., 2006). Of those that gave a stronger response to reward, the magnitude of IC cell activation was related to the magnitude of the reward (Metzger et al., 2006). Therefore, IC cells show convergent audio, visual, and attentional activation properties that could feasibly be used to direct MOC activation.

At the cortical level, deafening and partial hearing loss can result in multisensory plasticity (Allman et al., 2009; Meredith et al., 2012). Therefore, the integration of visual and somatosensory information with auditory input at the level of the IC may help to explain the appearance of normal synapses in pathological hearing conditions seen here. Accordingly, the incorporation of non-auditory input in the descending auditory pathway may prove a critical factor in understanding the extent and time course of neural reorganization that occurs following loss of afferent auditory input.

4.5. Conclusions

We have systematically mapped the tonotopic nature of the descending IC projection in normal hearing mice and quantified the

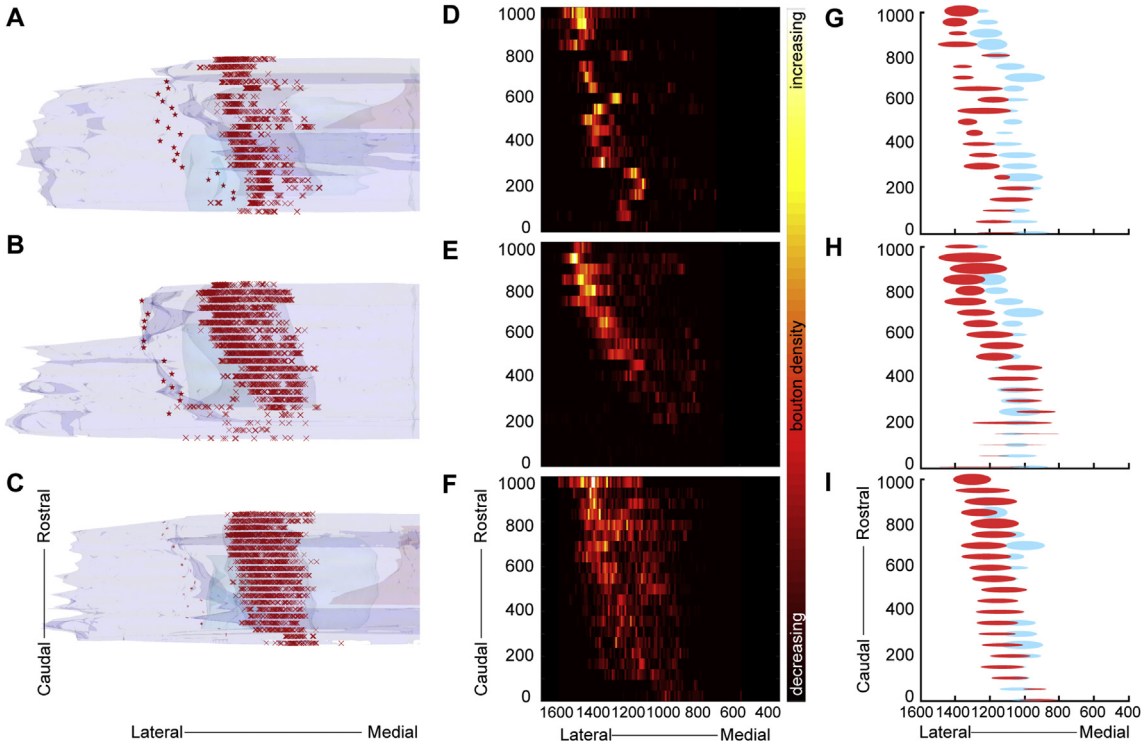

Fig. 12. Frequency organization of the descending terminal fields in individual 6-month old congenitally deaf Shaker2 mice. (A–C) 3-dimensional renderings of boutons (red crosses) in VNTB viewed from the dorsal aspect of the brain show their distribution through the superior olivary complex. (D–F) Heat maps of normalized data from each case show bouton density with respect to spread along the mediolateral and rostrocaudal axes. The density and spread of descending terminals in deaf cases appeared patchy in comparison to the hearing and hearing loss cases. (G–I) Plots of each case (red) showing relative bouton density (ellipse height) and mean ± SD (ellipse center and length, respectively), with the 11 kHz CBA/CaH (blue) plotted for reference. The terminal field of deaf cases appeared to be located laterally with respect to the normal hearing CBA/CaH at 11 kHz, but only the grand mean of the first animal (A, D, G) showed statistical significance ($p \leq 0.0001$). All deaf cases showed significantly greater variance than the normal hearing CBA/CaH at 11 kHz ($p < 0.05$).

pathologic distribution of these projections in mice with impaired hearing. MOC efferent neurons located medially receive high frequency input from the IC and project to basal, high frequency cochlear regions. MOC efferent neurons that are situated more medially receive progressively lower frequency input from the IC and project to progressively more apical cochlear regions (Guinan et al., 1984; Robertson et al., 1987; Brown, 1993). Thus the IC sends excitatory signals directly to frequency matched MOC efferents.

The differential patterns of tonotopic reorganization recorded in the two models of pathologic hearing (DBA/2 and *sh2/sh2* mice) are consistent with current ideas of stimulus-dependent refinement of tonotopy that is present prior to the onset of hearing (Gabriele et al., 2000; Leake et al., 2002; Kandler, 2004; Kandler et al., 2009). Axonal pruning that maintains frequency organization is dependent on normal, afferent input, as shown in animals reared under constant, sub-threshold shift inducing white noise (Werthat et al., 2008). The presence of auditory input after hearing onset is a critical time in axonal refinement (Werthat et al., 2008). The two mouse strains with pathological hearing utilized in this study allowed us to investigate the nature of such pruning in progressive frequency-specific hearing loss and in the absence of any sound input.

DBA/2 mice display progressive high frequency hearing loss, present at P11 (hearing onset). At one month of age, thresholds in the frequency region investigated here are elevated. Therefore, the refinement of the pre-existing tonotopic arrangement by axonal pruning could still occur (Kandler et al., 2009). As no significant change in variance in mediolateral terminal location across the rostrocaudal axis was evident when compared to normal hearing animals, our data support an input-dependent tonotopic refinement. The descending terminal redistribution is reminiscent of cortical plasticity, where topographic reorganization occurs after sensory damage. The preferential high frequency hearing loss in these animals is predictive of the medial location shift observed.

In the absence of afferent input, axonal pruning fails to occur, and the tonotopic organization resembles that seen prior to hearing onset (Gabriele et al., 2000). Consequently, the organization of descending IC input in the congenitally deaf *Shaker-2* mice matched what would be predicted prior to hearing onset. No mediolateral shift was observed compared to the normal hearing animals, although the greater variance in mediolateral location across the rostrocaudal axis suggests that an absence of afferent input impaired the axonal pruning that refines the pre-existing descending tonotopy.

It is difficult to assess the accuracy of mediolateral shifts in our hearing loss and deafness animals because one contributor to the variation is the difference in injection site location and tracer spread between animals. Nevertheless, we predict that the significantly greater variance seen in the deaf but not hearing loss animal reflects the influence of afferent input on axonal pruning. In this context, a number of predictions can be made with respect to terminal organization in different frequency regions in each of these animals. For example, in the congenitally deaf animal, we would expect tracer injections at any frequency to result in a greater terminal bouton spread due to impaired pruning. On the other hand, descending high frequency projections from the IC of a DBA/2 animal, with early onset high frequency hearing loss, are predicted to show an increased spread of terminal distribution similiar to that of deaf animals. IC projections to MOCs from the low frequency region might be expected to appear more like those of normal hearing mice because they have not yet been affected by hearing loss.

These small but significant changes in the descending terminal fields that accompany hearing loss and deafness could result in decreased gain control via improper MOC activation. The implication of this change is that precision of descending sources enabling selective suppression of “noise” is blurred. For humans, such changes could contribute to a difficulty understanding speech in noisy environments.

Conflicts of interest

None.

Role of authors

Both authors were involved in the design of the experiments, analyses of the data, and writing of the manuscript. KS conducted actual collection of data. Funding for the project was secured by DKR through grants and donations to the lab. Both authors approved the final version of the article.

Funding sources

UNSW APA, NHMRC 1080652, Oticon Foundation 12-1540, Walker Family Foundation, and gifts from Alan and Lynne Rydge, and Haydn and Sue Daw.

Acknowledgements

The authors gratefully acknowledge Katanyu Pongstaporn for his technical expertise in electron microscopy; Giedre Milikeviciute for sharing experimental tissue; Catherine Connelly for her critical input to the design and execution of stereotaxic injections in mice with hearing loss and deafness; and Dr Michael Muniak for sharing experimental tissue and providing valuable assistance with data analysis.

References

Adams, J.C., Wenthold, R.J., 1979. Distribution of putative amino acid transmitters, choline acetyltransferase and glutamate decarboxylase in the inferior colliculus. Neuroscience 4 (12), 1947–1951.
Allman, B.L., Keniston, L.P., Meredith, M.A., 2009. Adult deafness induces somatosensory conversion of ferret auditory cortex. Proc. Natl. Acad. Sci. 106 (14), 5925–5930.
Andeol, G., Guillaume, A., Micheyl, C., Savel, S., Pellieux, L., Moulin, A., 2011. Auditory efferents facilitate sound localization in noise in humans. J. Neurosci. 31 (18), 6759–6763.
Benson, T.E., Brown, M.C., 2006. Ultrastructure of synaptic input to medial olivocochlear neurons. J. Comp. Neurol. 499 (2), 244–257.
Beyer, L.A., Odeh, H., Probst, F.J., Lambert, E.H., Dolan, D.F., Camper, S.A., Kohrman, D., Raphael, Y., 2000. Hair cells in the inner ear of the pirouette and shaker 2 mutant mice. J. Neurocytol. 29 (4), 227–239.
Billups, B., 2005. Colocalization of vesicular glutamate transporters in the rat superior olivary complex. Neurosci. Lett. 382 (1–2), 66–70.
Blaesse, P., Ehrhardt, S., Friauf, E., Nothwang, H.G., 2005. Developmental pattern of three vesicular glutamate transporters in the rat superior olivary complex. Cell Tissue Res. 320 (1), 33–50.
Bogaerts, S., Clements, J.D., Sullivan, J.M., Oleskevich, S., 2009. Automated threshold detection for auditory brainstem responses: comparison with visual estimation in a stem cell transplantation study. BMC Neurosci. 10 (1), 1–7.
Bregman, A.S., 1994. Auditory Scene Analysis: the Perceptual Organization of Sound. The MIT Press, Cambridge, Massachusetts.
Brown, M., 2014. Single-unit labelling of medial olivocochlear neurons: the cochlear frequency map for efferent axons. J. Neurophysiol. 111 (11), 2177–2186.
Brown, M.C., 1989. Morphology and response properties of single olivocochlear fibers in the Guinea pig. Hear. Res. 40 (1–2), 93–109.
Brown, M.C., 1993. Fiber pathways and branching patterns of biocytin-labeled olivocochlear neurons in the mouse brainstem. J. Comp. Neurol. 337 (4), 600–613.
Brown, M.C., de Venecia, R.K., Guinan Jr., J.J., 2003. Responses of medial olivocochlear neurons. Specifying the central pathways of the medial olivocochlear reflex. Exp. Brain Res. 153 (4), 491–498.
Brown, M.C., Mukerji, S., Drottar, M., Windsor, A.M., Lee, D.J., 2013. Identification of inputs to olivocochlear neurons using transneuronal labeling with pseudorabies Virus (Prv). J. Assoc. Res. Otolaryngol. 14 (5), 703–717.
Caicedo, A., Herbert, H., 1993. Topography of descending projections from the inferior colliculus to auditory brainstem nuclei in the rat. J. Comp. Neurol. 328 (3), 377–392.

David, M., Lavandier, M., Grimault, N., 2015. Sequential streaming, binaural cues and Lateralization. J. Acoust. Soc. Am. 138 (6), 3500–3512.
Delano, P.H., Elgueda, D., Hamame, C.M., Robles, L., 2007. Selective attention to visual stimuli reduces cochlear sensitivity in chinchillas. J. Neurosci. 27 (15), 4146–4153.
Dragicevic, C.D., Aedo, C., Leon, A., Bowen, M., Jara, N., Terreros, G., Robles, L., Delano, P.H., 2015. The olivocochlear reflex strength and cochlear sensitivity are independently modulated by auditory cortex microstimulation. J. Assoc. Res. Otolaryngol. 16 (2), 223–240.
Faye-Lund, H., 1986. Projection from the inferior colliculus to the superior olivary complex in the albino rat. Anat. Embryol. 175 (1), 35–52.
Feliciano, M., Saldaña, E., Mugnaini, E., 1995. Direct projections from the rat primary auditory neocortex to nucleus sagulum, paralemniscal regions, superior olivary complex and cochlear nuclei. Audit. Neurosci. 1, 287–308.
Gabriele, M.L., Brunso-Bechtold, J.K., Henkel, C.K., 2000. Plasticity in the development of afferent patterns in the inferior colliculus of the rat after unilateral cochlear ablation. J. Neurosci. 20 (18), 6939–6949.
Groff, J.A., Liberman, M.C., 2003. Modulation of cochlear afferent response by the lateral olivocochlear system: activation via electrical stimulation of the inferior colliculus. J. Neurophysiol. 90 (5), 3178–3200.
Groh, J.M., Trause, A.S., Underhill, A.M., Clark, K.R., Inati, S., 2001. Eye position influences auditory responses in primate inferior colliculus. Neuron 29 (2), 509–518.
Guinan, J.J., Warr, B.W., Norris, B.E., 1983. Differential olivocochlear projections from lateral versus medial zones of the superior olivary complex. J. Comp. Neurol. 221 (3), 358–370.
Guinan, J.J., Warr, B.W., Norris, B.E., 1984. Topographic organization of the olivocochlear projections from the lateral and medial zones of the superior olivary complex. J. Comp. Neurol. 226 (1), 21–27.
Helfert, R.H., Bonneau, J.M., Wenthold, R.J., Altschuler, R.A., 1989. Gaba and glycine immunoreactivity in the Guinea pig superior olivary complex. Brain Res. 501 (2), 269–289.
Hultcranz, M., Spangberg, M., 1997. Pathology of the cochlea following a spontaneous mutation in DBA/2 mice. Acta Oto Laryng 117 (5), 689–695.
Irving, S., Moore, D.R., Liberman, M.C., Sumner, C.J., 2011. Olivocochlear efferent control in sound localization and experience-dependent Learning. J. Neurosci. 31 (7), 2493–2501.
Johnson, K.R., Zheng, Q.Y., Erway, L.C., 2000. A major gene affecting age-related hearing loss is common to at least ten inbred strains of mice. Genomics 70 (2), 171–180.
Kandler, K., 2004. Activity-dependent organization of inhibitory circuits: Lessons from the auditory system. Curr. Opin. Neurobiol. 14 (1), 96–104.
Kandler, K., Clause, A., Noh, J., 2009. Tonotopic reorganization of developing auditory brainstem circuits. Nat. Neurosci. 12 (6), 711–717.
Kawase, T., Delgutte, B., Liberman, M.C., 1993. Antimasking effects of the olivocochlear reflex. Ii. Enhancement of auditory-nerve response to masked tones. J. Neurophysiol. 70 (6), 2533–2549.
Kelly, J.B., Caspary, D.M., 2005. Pharmacology of the inferior colliculus. In: Winer, J.A., Schreiner, C.E. (Eds.), The Inferior Colliculus. Springer New York, New York, NY, pp. 248–281.
Kumar, U.A., Vanaja, C.S., 2004. Functioning of olivocochlear bundle and speech perception in noise. Ear Hear. 25 (2), 142–146.
Leake, P.A., Snyder, R.L., Hradek, G.T., 2002. Postnatal refinement of auditory nerve projections to the cochlear nucleus in cats. J. Comp. Neurol. 448 (1), 6–27.
Lee, D.J., Cahill, H.B., Ryugo, D.K., 2003. Effects of congenital deafness in the cochlear nuclei of Shaker-2 mice: an ultrastructural analysis of synapse morphology in the endbulbs of held. J. Neurocytol. 32 (3), 229–243.
Liang, Y., Wang, A., Belyantseva, I.A., Anderson, D.W., Probst, F.J., Barber, T.D., Miller, W., Touchman, J.W., Jin, L., Sullivan, S.L., Sellers, J.R., Camper, S.A., Lloyd, R.V., Kachar, B., Friedman, T.B., Fridell, R.A., 1999. Characterization of the human and mouse unconventional myosin Xv genes responsible for hereditary deafness Dfnb3 and shaker 2. Genomics 61 (3), 243–258.
Liberman, M.C., 1988. Response properties of cochlear efferent neurons: monaural Vs. Binaural stimulation and the effects of noise. J. Neurophysiol. 60 (5), 1779–1798.
Liberman, M.C., 1989. Rapid assessment of sound-evoked olivocochlear feedback: suppression of compound action potentials by contralateral sound. Hear. Res. 38 (1–2), 47–56.
Liberman, M.C., Brown, M.C., 1986. Physiology and anatomy of single olivocochlear neurons in the Cat. Hear. Res. 24 (1), 17–36.
Liberman, M.C., Maison, S.F., 2014. Shelter from the glutamate storm: loss of olivocochlear efferents increases cochlear nerve degeneration during aging. J. Acoust. Soc. Am. 135 (4), 2384–2384.
Lukas, J.H., 1981. The role of efferent inhibition in human auditory attention: an examination of the auditory brainstem potentials. Int. J. Neurosci. 12 (2), 137–145.
Maison, S.F., Usubuchi, H., Liberman, M.C., 2013. Efferent feedback minimizes cochlear neuropathy from moderate noise exposure. J. Neurosci. 33 (13), 5542–5552.
Malmierca, M.S., Lebeau, F.E.N., Rees, A., 1996. The topographical organization of descending projections from the central nucleus of the inferior colliculus in Guinea pig. Hear. Res. 93 (1–2), 167–180.
Malmierca, M.S., Ryugo, D.K., 2010. Descending connections to the midbrain and brainstem. In: Winer, J.A., Schreiner, C.E. (Eds.), The Auditory Cortex. Springer-Verlag, New York, pp. 189–208.
Malmierca, M.S., Ryugo, D.K., 2011. The mouse auditory system. In: Watson, C., Paxinos, G., Puelles, L. (Eds.), The Mouse Nervous System. Academic Press, New York, pp. 607–645.
May, B.J., Budelis, J., Niparko, J.K., 2004. Behavioral studies of the olivocochlear efferent system: Learning to listen in noise. Arch. Otolaryngol. Head. Neck Surg. 130 (5), 660–664.
Meredith, M.A., Keniston, L.P., Allman, B.L., 2012. Multisensory dysfunction accompanies crossmodal plasticity following adult hearing impairment. Neuroscience 214, 136–148.
Merzenich, M.M., Reid, M.D., 1974. Representation of the cochlea within the inferior colliculus of the Cat. Brain Res. 77 (3), 397–415.
Metzger, R.R., Greene, N.T., Porter, K.K., Groh, J.M., 2006. Effects of reward and behavioral context on neural activity in the primate inferior colliculus. J. Neurosci. 26 (28), 7468–7476.
Middlebrooks, J.C., Onsan, Z.A., 2012. Stream segregation with high spatial acuity. J. Acoust. Soc. Am. 132 (6), 3896–3911.
Morin, L.P., Studholme, K.M., 2014. Retinofugal projections in the mouse. J. Comp. Neurol. 522 (16), 3733–3753.
Mulders, W.H., Seluakumaran, K., Robertson, D., 2010. Efferent pathways modulate hyperactivity in inferior colliculus. J. Neurosci. 30 (28), 9578–9587.
Mulders, W.H.A.M., Robertson, D., 2000a. Effects on cochlear responses of activation of descending pathways from the inferior colliculus. Hear. Res. 149 (1–2), 11–23.
Mulders, W.H.A.M., Robertson, D., 2000b. Evidence for direct cortical innervation of medial olivocochlear neurones in rats. Hear. Res. 144 (1–2), 65–72.
Mulders, W.H.A.M., Robertson, D., 2002. Inputs from the cochlea and the inferior colliculus converge on olivocochlear neurones. Hear. Res. 167 (1–2), 206–213.
Muniak, M.A., Mayko, Z.M., Ryugo, D.K., Portfors, C.V., 2012. Preparation of an awake mouse for recording neural responses and injecting tracers. J. Vis. Exp. 64, e3755.
Oatman, L.C., 1971. Role of visual attention on auditory evoked potentials in unanesthetized cats. Exp. Neurol. 32 (3), 341–356.
Oatman, L.C., 1976. Effects of visual attention on the intensity of auditory evoked potentials. Exp. Neurol. 51 (1), 41–53.
Oatman, L.C., Anderson, B.W., 1977. Effects of visual attention on tone burst evoked auditory potentials. Exp. Neurol. 57 (1), 200–211.
Ota, Y., Oliver, D.L., Dolan, D.F., 2004. Frequency-specific effects on cochlear responses during activation of the inferior colliculus in the Guinea pig. J. Neurophysiol. 91 (5), 2185–2193.
Perrot, X., Ryvlin, P., Isnard, J., Guenot, M., Catenoix, H., Fischer, C., Mauguiere, F., Collet, L., 2006. Evidence for corticofugal modulation of peripheral auditory activity in humans. Cereb. Cortex 16 (7), 941–948.
Popelar, J., Mazelová, J., Syka, J., 2002. Effects of electrical stimulation of the inferior colliculus on 2f1−F2 distortion product otoacoustic emissions in anesthetized Guinea pigs. Hear. Res. 170 (1–2), 116–126.
Porter, K.K., Metzger, R.R., Groh, J.M., 2007. Visual- and saccade-related signals in the primate inferior colliculus. Proc. Natl. Acad. Sci. U. S. A. 104 (45), 17855–17860.
Probst, F.J., Fridell, R.A., Raphael, Y., Saunders, T.L., Wang, A., Liang, Y., Morell, R.J., Touchman, J.W., Lyons, R.H., Noben-Trauth, K., Friedman, T.B., Camper, S.A., 1998. Correction of deafness in *Shaker-2* mice by an unconventional myosin in a bac transgene. Science 280 (5368), 1444–1447.
Rajan, R., 1988a. Effect of electrical stimulation of the crossed olivocochlear bundle on temporary threshold shifts in auditory sensitivity. I. Dependence on electrical stimulation parameters. J. Neurophysiol. 60 (2), 549–568.
Rajan, R., 1988b. Effect of electrical stimulation of the crossed olivocochlear bundle on temporary threshold shifts in auditory sensitivity. Ii. Dependence on the level of temporary threshold shifts. J. Neurophysiol. 60 (2), 569–579.
Rajan, R., 1990. Electrical stimulation of the inferior colliculus at low rates protects the cochlea from auditory desensitization. Brain Res. 506 (2), 192–204.
Rajan, R., 1995. Involvement of cochlear efferent pathways in protective effects elicited with binaural Loud sound exposure in cats. J. Neurophysiol. 74 (2), 582–597.
Robertson, D., 1984. Horseradish peroxidase injection of physiologically characterized afferent and efferent neurones in the Guinea pig spiral Ganglion. Hear. Res. 15 (2), 113–121.
Robertson, D., Anderson, C.-J., Cole, K.S., 1987. Segregation of efferent projections to different turns of the Guinea pig cochlea. Hear. Res. 25 (1), 69–76.
Rose, J.E., Greenwood, D.D., Goldberg, J.M., Hind, J.E., 1963. Some discharge characteristics of single neurons in the inferior colliclulus of the cat. I. Tonotopic organization, relation of spike-counts to tone intensity, and firing patterns of single elements. J. Neurophysiol. 26 (2), 294–320.
Roth, G.L., Aitken, L.M., Anderson, R.A., Merzenich, M.M., 1978. Some features of the spatial organization of the central nucleus of the inferior colliculus of the cat. J. Comp. Neurol. 182, 661–680.
Ryan, A., Miller, J., 1977. Effects of behavioral performance on single-unit firing patterns in inferior colliculus of the rhesus monkey. J. Neurophysiol. 40 (4), 943–956.
Ryan, A., Miller, J., Pfingst, B., Martin, G., 1984. Effects of reaction time performance on single-unit activity in the central auditory pathway of the rhesus macaque. J. Neurosci. 4 (1), 298–308.
Ryugo, D.K., 2010. In: Ryugo, D.K., Popper, A.N., Fay, R.R. (Eds.), Auditory and Vestibular Efferents. Springer-Verlag, New York.
Saint Marie, R.L., 1996. Glutamatergic connections of the auditory midbrain: selective uptake and axonal transport of D-[3h]Aspartate. J. Comp. Neurol. 373 (2),

255–270.
Scates, K.W., Woods, C.I., Azeredo, W.J., 1999. Inferior colliculus stimulation and changes in 2f1−F2 distortion product otoacoustic emissions in the rat. Hear. Res. 128 (1–2), 51–60.
Syka, J., Radil-weiss, T., 1973. Acoustical responses of inferior colliculus neurons in rats influenced by sciatic nerve stimulation and light flashes. Int. J. Neurosci. 5 (5), 201–206.
Tawil, R.N., Saade, N.E., Bitar, M., Jabbur, S.J., 1983. Polysensory interactions on single neurons of Cat inferior colliculus. Brain Res. 269 (1), 149–152.
Thompson, A.M., Thompson, G.C., 1993. Relationship of descending inferior colliculus projections to olivocochlear neurons. J. Comp. Neurol. 335 (3), 402–412.
Tong, H., Kopp-Scheinpflug, C., Pilati, N., Robinson, S.W., Sinclair, J.L., Steinert, J.R., Barnes-Davies, M., Allfree, R., Grubb, B.D., Young, S.M., Forsythe, I.D., 2013. Protection from noise-induced hearing loss by Kv2.2 potassium currents in the central medial olivocochlear system. J. Neurosci. 33 (21), 9113–9121.
Vetter, D.E., Adams, J.C., Mugnaini, E., 1991. Chemically distinct rat olivocochlear neurons. Synapse 7 (1), 21–43.
Vetter, D.E., Saldaña, E., Mugnaini, E., 1993. Input from the inferior colliculus to medial olivocochlear neurons in the rat: a double label study with pha-L and cholera toxin. Hear. Res. 70 (2), 173–186.
Wang, X., Robertson, D., 1997. Two types of actions of norepinephrine on identified auditory efferent neurons in rat brain stem slices. J. Neurophysiol. 78 (4), 1800–1810.
Wang, Y., Manis, P.B., 2006. Temporal coding by cochlear nucleus bushy cells in Dba/2j mice with early onset hearing loss. J. Assoc. Res. Otolaryngol. 7 (4), 412–424.
Werthat, F., Alexandrova, O., Grothe, B., Koch, U., 2008. Experience-dependent refinement of the inhibitory axons projecting to the medial superior olive. Dev. Neurobiol. 68 (13), 1454–1562.
Willott, J.F., Demuth, R.M., Lu, S.M., 1984. Excitability of auditory neurons in the dorsal and ventral cochlear nuclei of Dba/2 and C57bl/6 mice. Exp. Neurol. 83 (3), 495–506.
Winslow, R.L., Sachs, M.B., 1987. Effect of electrical stimulation of the crossed olivocochlear bundle on auditory nerve response to tones in noise. J. Neurophysiol. 57 (4), 1002–1021.
Winslow, R.L., Sachs, M.B., 1988. Single-tone intensity discrimination based on auditory-nerve rate responses in backgrounds of quiet, noise, and with stimulation of the crossed olivocochlear bundle. Hear. Res. 35 (2–3), 165–190.
Woods, C.I., Azeredo, W.J., 1999. Noradrenergic and serotonergic projections to the superior olive: potential for modulation of olivocochlear neurons. Brain Res. 836 (1–2), 9–18.
Xiao, Z., Suga, N., 2002. Modulation of cochlear hair cells by the auditory cortex in the mustached bat. Nat. Neurosci. 5 (1), 57–63.
Yao, W., Godfrey, D.A., 1995. Immunohistochemistry of muscarinic acetylcholine receptors in rat superior olivary complex. Hear. Res. 89 (1–2), 76–85.
Yao, W., Godfrey, D.A., 1997. Densitometric evaluation of markers for cholinergic transmission in rat superior olivary complex. Neurosci. Lett. 229 (1), 21–24.
Yao, W., Godfrey, D.A., 1998. Immunohistochemical evaluation of cholinergic neurons in the rat superior olivary complex. Microsc. Res. Tech. 41 (3), 270–283.
Ye, Y., Machado, D.G., D.O., K., 2000. Projection of the marginal shell of the anteroventral cochlear nucleus to olivocochlear neurons in the cat. J. Comp. Neurol. 420 (1), 127–138.
Zhang, W., Dolan, D.F., 2006. Inferior colliculus stimulation causes similar efferent effects on ipsilateral and contralateral cochlear potentials in the Guinea pig. Brain Res. 1081 (1), 138–149.
Zheng, Q.Y., Johnson, K.R., Erway, L.C., 1999. Assessment of hearing in 80 inbred strains of mice by abr threshold analyses. Hear Res. 130 (1–2), 94–107.